JOURNAL OF MATERIALS SCIENCE 12 (1977) 2235–2240

Phosphate conversion coatings on steel

J. BOGI, R. MACMILLAN
Department of Materials Science, The New South Wales Institute of Technology, Sydney, Australia.

A mechanism for the formation of crystalline phosphate conversion coatings on steel is proposed from the results of this investigation. X-ray diffraction results identify the crystal types formed from both Zn and Mn phosphating baths. The effect of process parameters, such as metal surface finish and soluble iron content of the phosphate bath, on crystal size and surface layering are discussed. Differential thermal analysis shows the water of crystallization of the phosphate precipitates to be driven off at about 325° C with corresponding contraction and fracture of the surface crystal. Corrosion data was determined and correlated with the crystal morphology. Scanning electron micrographs were taken of the various crystal systems produced to confirm conclusions drawn from the data collected.

1. Introduction

Inorganic conversion coatings, in particular phosphate coatings, have been in use commercially for over 60 years as a corrosion protection system for ferrous metals [1]. Crystalline coatings of iron phosphate, manganese phosphate or zinc phosphate are deposited from solution on to the ferrous metal surface by immersion in a sequence of degreasing, pickling and phosphating baths with appropriate rinses. More recent developments, using accelerating agents such as nitrates, have made spraying applications possible, with obvious advantages for large articles.

The phosphate conversion coating only affords partial protection to the surface and is normally used in conjunction with a sealant such as oil, grease or wax. In many commercial applications the phosphate coating offers a suitable mechanical key for paints and enamels.

Little has been published on the fundamental mechanism of the process. The possibility of the use of dual phosphating systems has received no theoretical attention.

W. Machu [2–6] considered phosphating as an electrochemical process and made a significant contribution in clarifying the mechanism. On this basis he was able to explain the effects of surface treatments, oxidizing agents and the rates of reaction. He also proposed [4] that the precipitation took place at cathodic sites on the metal surface due to pH changes caused by the discharge of hydrogen ions.

Wulfson [7] on the other hand postulated the deposition occurring at anodic sites due to the high metallic ion concentration in anodic regions.

Krutikov [8] suggested that formation of a thin film of phosphate at anodic sites which then became cathodic. Discharge of hydrogen at these cathodes leads to the precipitation of phosphate crystal at the cathodic site.

Ghali and Potvin [9] proposed the existence of several passivating steps, namely the amorphous precipitation, crystallization and growth, followed by crystalline reorganization. They also confirmed the crystal structure of zinc phosphate coatings to be hopeite $Zn_3(PO_4)_2 . 4H_2O$ as proposed by several authors [10].

The purpose of this study was to investigate phosphating processes involving zinc phosphate and manganese phosphate coatings in an attempt to (i) clarify the mechanism of coating formation, (ii) identify the coating structures, (iii) investigate the effects of process parameters and (iv) to study the possibility of dual phosphating processes.

2. Experimental

2.1. Coating conditions

Phosphate coatings were produced on free machining steel buttons of the exact dimension of the Philips X-ray diffractometer PW1050 sample

holder, as well as on 5 cm^2 steel panels.

Commercial zinc phosphate and manganese phosphate solutions of the following compositions were used: (i) Mn–Fe: 0.4% $Fe(H_2PO_4)_2$ + 1.2% $Mn(H_2PO_4)_2$; (ii) Zn: 1.0% $Zn(H_2PO_4)_2$.

The steel was pickled in 33 vol% HCl after abrading and polishing to 600 finish. Subsequent rinsing in hot and cold water was carried out prior to phosphating.

In the phosphating bath the deposition of precipitated "dust" on the specimen was prevented by using the steel itself as the stirrer, with a magnetic stirrer rotating in the opposite direction on the bottom of the bath. The temperature of the phosphate baths was maintained at 95 ± 0.5° C and to avoid depletion of the ion concentration in the bath a fresh solution was used for each sample of steel treated.

2.2. Coating investigations

(i) Non-destructive studies using X-ray diffraction and X-ray fluorescence were carried out to identify the nature of the crystalline coating. (ii) Scanning electron microscope investigations of the development of the phosphate crystals and the nature of the coverage were made. (iii) Chemical analysis of the coating was carried out after dissolving the coating in nitric acid and analysing via atomic absorption spectrophotometry. (iv) Thermal gravimetric analysis (TGA) and differential thermal analysis (DTA) were used to determine the effect of temperature on the waters of crystallisation in the crystal and the subsequent effect on the corrosion protection. (v) Relative corrosion protection was noted by the rate of the appearance of rust when specimens were stored in a constant humidity salt chamber.

3. Crystallographic studies

X-ray diffraction data were obtained directly from the phosphated steel buttons as well as from crystals scraped from the surface of the phosphated flat mild-steel plates. The unit cell dimensions and structure were confirmed by precision camera photographs.

The results of Ghali and Potvin [9] for zinc phosphated steel were confirmed in that crystals of phosphophyllite, a mixed iron and zinc phosphate $(Zn_xFe_y)_3(PO_4)_2.4H_2O$ and hopeite, a zinc phosphate $Zn_3(PO_4)_2.4H_2O$ were identified (Table I). The former structure is predominant from short immersion periods with the zinc phosphate deposit occurring during the crystal growth stage.

TABLE I Zinc phosphate coating

Experimental *d* (Å)	Hopeite [10] *d* (Å)
9.10	9.10
5.30	5.30
5.06	5.10
4.58	4.59
4.44	4.40
3.99	4.01
3.46	3.47
3.39	3.40
2.85	2.85
2.65	2.63
2.61	2.52
2.54	2.42
2.34	2.33
2.28	2.27
2.098	2.09
2.000	2.00
1.938	1.94
1.824	1.82

TABLE II Manganese phosphate coating

Steel button *d* (Å)	Steel panel *d* (Å)	Hureaulite [11] *d* (Å)
8.75	8.75	8.62
8.10	8.10	8.01
6.30	6.30	6.30
5.98	6.02	5.98
4.72	4.38	4.68
4.56	4.74	4.50
4.38	4.56	4.35
4.12	4.07	4.05
3.77	3.80	3.77
3.65	3.66	3.64
3.40	3.42	3.40
3.25	3.28	3.25
3.19	3.20	3.18
3.15	3.15	3.14
3.07	3.08	3.06
3.04	3.05	3.01
3.00	3.00	2.99
2.92	2.91	2.902
2.875	2.88	2.860
2.78	2.78	2.766
2.73	2.73	2.722
2.70	2.70	2.691
2.63	2.63	2.620
2.59	2.59	2.580
2.555	2.56	2.553

Manganese phosphate coatings previously unidentified, showed only the mixed manganese iron phosphate with the "Hureaulite" crystal structure,

similar to that quoted by Fisher [12] for the mineral Hureaulite (Table II).

Chemical analysis of the manganese phosphate crystals precipitated from solutions with variable iron content in the bath showed the crystals to contain a larger Fe content when deposited from a fresh bath with a high iron concentration.

An identical structure was maintained with a greater percentage of manganese in the lattice as the iron concentration in the bath was depleted.

The ratio of Mn–Fe in the crystal may vary as shown in Table III but the total percentage of Mn + Fe (39.1%) compares well with the theoretical value of 38 ± 0.4%.

Thermogravimetric analysis showed a 10% weight loss at 325° C. Gravimetric determinations on previously dried crystals confirmed this weight loss of 10%. The suggested structure of the manganese phosphate is therefore $(Mn, Fe)_5H_2(PO_4)_4 . 4H_2O$ [11].

TABLE III

Solution Analysis	Coating Analysis		
% Fe in Solution	% Fe	% Mn	Total Mn + Fe
0.125	5.0	35.1	40.1
0.150	5.2	34.1	39.3
0.175	6.3	33.0	39.3
0.200	8.4	30.6	39.0
0.225	11.5	27.5	39.0

4. Scanning electron microscopy

Low magnification scanning electron microscopy was used to illustrate the various phases of phosphate deposition. Acid-pickling to remove surface scale (Fig. 1) has resulted in the selective etching of sulphide inclusions in the steel in question. This allows the easy identification of anodic and cathodic sites.

Increasing immersion times in manganese phosphate baths, (Fig. 2), shows the formation of a fine amorphous manganese iron phosphate depositing uniformly over the surface with no apparent preference for anodic site reaction. Deposition at cathodic regions results from the pH shift due to the discharge of hydrogen ions. With Zn phosphate-immersion (Fig. 3) crystal growth from the edges of etch pits was extremely rapid with very little growth on the plateaus. Eventually due to the blocking of these anodic sites the plateau becomes anodic and the coverage is increased, (Fig. 4). Precipitation at anodic sites results from the high concentration of metal ions at these sites due to dissolution processes. This would suggest the deposition of a mixed iron and zinc phosphate in the early stages of precipitation.

Both zinc and manganese phosphate coatings remain porous with exposed metallic substrate remaining as centres for subsequent corrosive attack. The best protection is achieved when the surface is covered by a uniform fine crystalline

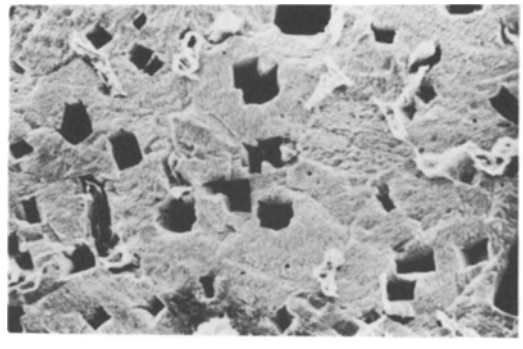

Figure 1 Acid-pickled steel surface.*

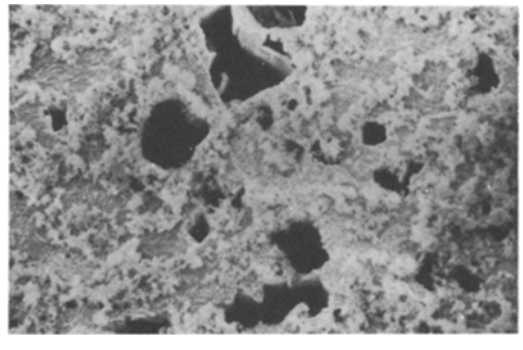

Figure 2 Manganese phosphate deposit.*

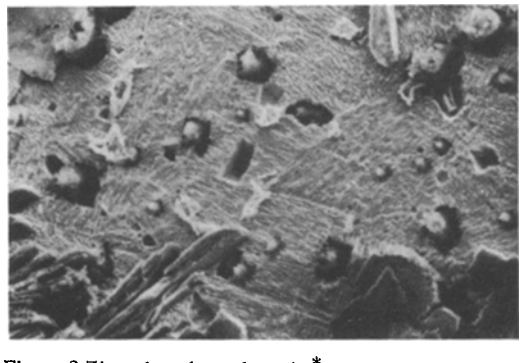

Figure 3 Zinc phosphate deposit.*

* Original magnification 640 ×. Reduced in reproduction to 76% original size.

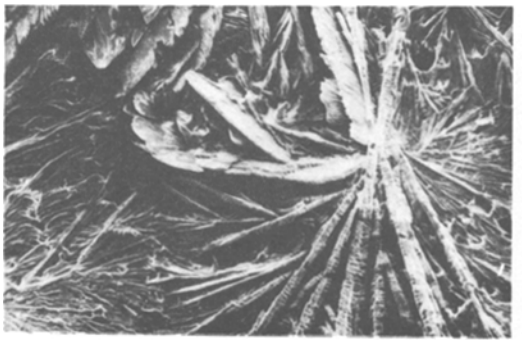

Figure 4 Growth of zinc phosphate crystals.*

Figure 5 Manganese phosphate crystals on rough abraded surface.*

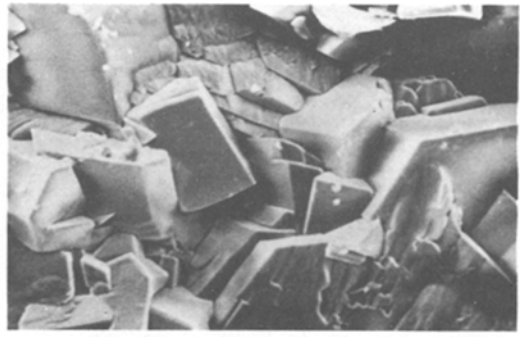

Figure 6 Manganese phosphate crystals on acid pickled abraded surface.*

Figure 7 Manganese phosphate crystals deposit from impurity nucleii.*

layer with few areas of exposed substrate. Substrate surface preparation prior to phosphating is a most important factor governing the quality of the protective coating.

Extremely rough surfaces, e.g. heavily abraded or grit-blasted, offer a large number of high surface-energy sites which are extremely reactive in the phosphoric acid solution as well as supplying a large number of nucleation centres. Due to the excessive roughness the crystals are irregular, and fine, with few areas of the substrate left exposed (Fig. 5).

Pickling prior to phosphating of the rough surface yields a smooth surface of low reactivity. The phosphate crystals are large and the protection inferior (Fig. 6).

The presence of solid impuriteis (dust etc.) on the work surface after pickling results in the formation of coarse crystals by supplying centres of nucleation (Fig. 7). These artificial nucleii may be removed by simply wiping the work surface to produce fine uniform crystals with superior protection (Fig. 8).

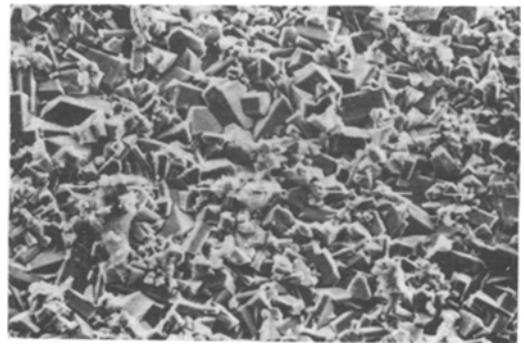

Figure 8 Fine crystals of manganese phosphate after removing the fine solid impurities by wiping.*

A smoother polished surface with low surface reactivity leads to a fine crystalline deposit with superior protection qualities (Fig. 9).

Thus the topography of the work surface is a most important factor governing the nature of the protective coating in that the size and distribution of the crystals defines the quality of the protection. This nature of the coating is a function of the

* Original magnification 640 ×. Reduced in reproduction to 76% original size.

Figure 9 Manganese phosphate deposit on low reactivity polished surface.†

Figure 10 Fracture of crystals caused by heating.†

reactivity of the surface and the number and distribution of the available nucleation sites.

Phosphate coatings are known to lose their protective qualities when used at high temperatures. Fig. 10 shows the crystals heated to above 325° C. Shrinkage has occurred along the growth axis due to the loss of water of crystallization with a corresponding decrease in the protection.

5. Discussion

The results of this study allow us to postulate the mechanism of the formation of inorganic phosphate conversion coatings in steel. Electrochemical attack of the metal surface on immersion in the phosphoric acid medium results in the formation of a soluble primary metal phosphate.

$$Me^{*} + 2H_3PO_4 \rightarrow Me(H_2PO_4)_2 + H_2\uparrow$$

Any surface oxide will also be dissolved:

$$MeO + 2H_3PO_4 \rightarrow Me(H_2PO_4)_2 + H_2O$$

The corresponding pH change causes an equilibrium shift to the more insoluble secondary phosphate.

$$Me(H_2PO_4)_2 \rightleftarrows MeHPO_4 + H_3PO_4$$

Further depletion of hydrogen ions causes a dissociation to the insoluble tertiary phosphate according to

$$3MeHPO_4 \rightleftarrows Me_3(PO_4)_2\downarrow + H_3PO_4$$

As the reactions are taking place at the metal surface, involving continuous dissolution of the substrate, coatings of mixed metal in content are likely. Deposition will also cease should the disolution process cease.

In the case of zinc phosphate the deposition and crystal growth takes place at anodic sites due to the production of metal ions at the anode. Therefore the zinc phosphate in solution is behaving as a typical anodic inhibitor in that the precipitate formed at the anodic site is a mixed zinc-iron phosphate resulting from the high concentration of metal ions in the anodic region. Further electrochemical attack is stimulated by the depletion of ion content in the anodic region by the nucleation of crystals of phosphyllite. As the anodes become covered with crystallites the attack on the substrate becomes more uniform and the deposition results in a crystal growth period during which the zinc phosphate (hopeite) predominates. This step follows the general reactions outlined above and is not influenced by large concentration of ferrous ions. The growth state is therefore pH controlled.

Uniform crystalline coatings of mangenese–iron phosphate are deposited at cathodic sites due to the change of pH at the metal solution interface. Ferrous ions produced at the surface diffuse slowly into the solution and some migrate to the cathodic region and precipitate as the tertiating mixed metal phosphate due to the pH shifts caused by the continued electrochemical attack of the metal surface. The crystals whilst varying in Mn/Fe ratio remain essentially of one type with the Hureaulite structure. We suggest,

$$Me + 2H_3PO_4 \rightarrow Me(H_2PO_4)_2 + H_2\uparrow$$

$$6\,Me(H_2PO_4)_2 \rightarrow 6\,MeHPO_4 + 6H_3PO_4$$

The $MeHPO_4$ is slightly soluble and with further pH changes, will form $Me_5H_2(PO_4)_4$ by either,

*Me = Mn + Fe

† Original magnification 640 ×. Reduced in reproduction to 76% original size.

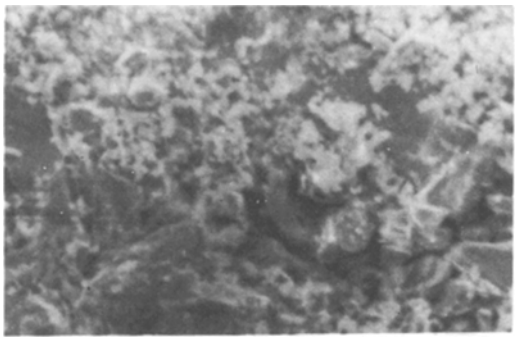

Figure 11 Dual phosphating; zinc phosphate on manganese phosphate (original magnification 640 ×). Reduced in reproduction to 76% original size.

$$5MeHPO_4 \rightarrow Me_5H_2(PO_4)_4 \cdot 4H_2O + H_3PO_4$$

$$6MeHPO_4 \rightarrow 2Me_3(PO_4)_2 + 2H_3PO_4.$$

$$2H_3PO_4 + 5Me_3(PO_4)2 \rightarrow 3Me_5H_2(PO_4)_4 \cdot 4H_2O$$

The importance of the size and distribution of the phosphate crystals on the surface of the substrate on the resultant corrosion protection has been illustrated.

We propose that difficulties in controlling the size and distribution of the crystalline coating can, however, be overcome by the use of a two-state phosphating process (Fig. 11). By initially depositing at cathodic regions and subsequent precipitation of a zinc-phosphate coating which will deposit in the steel anodic regions left exposed by the incomplete primary coat. Excellent protection is afforded the ferrous metal in this manner and specimen have been stored for a year without any visible signs of corrosion.

Corrosion protection is not improved by applying the dips in the reverse order due to the mechanism for the manganese phosphate deposition. Cathodic deposition will not occur on the substrate exposed between the zinc phosphate crystals.

References

1. T. W. COSLETT, British Patent 8667 and U.S. Patent 870937.
2. W. MACHU, *Korros. Metallschutz* **17** (1941) 157.
3. *Idem, Die Ernahrungsindustrie* **70** (1968) 549.
4. *Idem, Werkstoffe Korros.* **14** (1963) 566.
5. *Idem, ibid* **14** (1963) 273.
6. *Idem, Neue Hutte* **14** *Jg. Heft* 4 (1969) 238.
7. WULFSON and RABINOVICH Korro*siya I Borbasnei* **3** (1937) 363.
8. A. F. KRUTIKOV, *Zh. Prikl. Khim.* **37** (1964) 1462.
9. E. L. GHALI and R. J. A. POTVIN; *Corrosion Sci.* **12** (1972) 583.
10. ASTM Card No. 1–0964.
11. ASTM Card No. 16–383.
12. FISHER, *Am. Min.* **49** (1964) 398.

Received 28 January and accepted 24 February 1977.